

# Theoretical investigation of parameters influence on the performance of the metamaterial absorber and the design of the broadband absorption

BEN-XIN WANG<sup>a,\*</sup>, YUANHAO HE<sup>a</sup>, CHAO TANG<sup>a</sup>, QINGSHAN NIU<sup>a</sup>, FUWEI PI<sup>b,\*</sup>

<sup>a</sup>*School of Science, Jiangnan University, Wuxi 214122, China*

<sup>b</sup>*State Key Laboratory of Food Science and Technology, School of Food Science and Technology, Jiangnan University, Wuxi 214122, China*

---

Metamaterial-based absorbers have recently attracted considerable attention. Unfortunately, there are some differences between measurements and simulations, the underlying mechanisms for these behaviors have not yet been unraveled. A detailed understanding of the origin of these discrepancies is essential for optimizing the metamaterial absorber. Herein, we first study the influence of parameters on the performance of the absorber. The influence of parameters on the absorption performance can be summarized as three points. Immediately following, the practicability of the investigation is discussed by choosing two typical examples. Finally, according to the frequency-dependent parameters, three design strategies are summarized to obtain broadband absorbers.

(Received September 27, 2019; accepted August 18, 2020)

*Keywords:* Metamaterial, Perfect absorber, Terahertz, Broadband absorption

---

## 1. Introduction

Metamaterials, with the sub-wavelength scale unit cell, have attracted intense attention due to their exotic properties that are unavailable in nature, such as invisibility cloaking [1], perfect lensing [2] and negative index of refraction [3]. Many kinds of structures have been proposed for the landmark predictions of metamaterial theory [1]-[5]. In most device applications, such as filter, switch, modulator, sensor, the absorption loss of the metamaterials often degrades their performance. For an artificial light absorber, however, the absorption loss becomes useful and could be significantly enhanced by proper design of the structure.

The first perfect metamaterial absorber, having the measured absorptivity of about 88%, composed of a metallic split ring and a cut wire separated by a dielectric layer was demonstrated by Landy et al. [6]. Since then, metamaterial-based perfect absorbers have received considerable attention and many metamaterial absorbers have been proposed [7]-[17]. Unfortunately, all these efforts share the common shortcoming of narrow absorption bandwidth, which greatly hampers their practical applications. In practical applications, it is desirable to have perfect absorption over broader spectral bands. An effective method to broaden the absorption bandwidth is to make the metamaterial units resonate at several neighboring frequencies. Following this strategy, broadband or multi-band absorbers have been demonstrated in a wide frequency region ranging from microwave to optics [18]-[36]. For example, Cui et al. [18] demonstrated the broadband absorber by utilizing the

multiplexed plasmonic nanostructures in the infrared region. Shen et al. [20] presented the triple-band microwave absorber based on three nested closed-ring resonators. Grant et al. [21] achieved the bandwidth broadening by stacking multiple different sized metallic patterns.

It is noted that, however, the measured results (such as resonance frequency, absorption bandwidth as well as the absorption strength) are different from the simulated values. These small discrepancies are attributed to the fabrication tolerances (i.e., the change of the geometrical parameters) [18]-[30]. But the researchers did not clarify how the structure parameters affect the absorption performance of the absorber. Particularly, to date, the influence of the geometrical parameters on the performance of the absorber has yet to be addressed in detail. Therefore to comprehensively understand the absorption property of the metamaterial absorber, it is urgently necessary to investigate how the structure parameters affect its absorption performance.

This paper is dedicated to the systematically study the dependence of the absorption performance on the parameters change and explain the discrepancies between the measurements and simulations. With this goal in mind, the rest of this paper is organized as follows: In Section II, we first present a metamaterial absorber formed by a patterned metallic strip and a metallic ground plane separated by a dielectric layer. The reason for choosing the metallic strip structure in this study is that it is simple and easy to design and fabricate compared with the other metamaterial absorbers. The large light absorption of the metamaterial is attributed to the coupling of the electric

and magnetic resonances, and understanding of such the absorption mechanism is illustrated by investigating the electric and the magnetic field distributions at the absorption maximum. Moreover, in Section III, we systematically study the dependence of the absorption spectra on the parameters change of the absorber. It is found that the influence of the geometrical parameters on the performance of the absorber can be divided into three categories: (1) the absorber frequency mainly depends on the length and width of the metallic strip, the dielectric constant and dielectric layer thickness; and (2) the absorption strength is primarily determined by the dielectric constant and the dielectric layer thickness; while (3) the metallic conductivity and the metallic layer thickness as well as the lattice period have negligible influence on the absorption performance. Our demonstration can provide useful advice and guidance on how to optimize and design the metamaterial absorber and explain the discrepancies between the measurements and simulations. In the last part of this section, the practicability of the study is discussed by choosing two disagreement examples. Moreover, in Section IV, we summarize three design strategies to achieve the broadband absorbers based on the frequency-dependent structure parameters. The mechanism of the broadband absorbers originates from the overlapping of two different but similar frequencies. Finally, Section V concludes the paper.

## 2. Design of metamaterial absorber

The unit cell of the absorber structure is illustrated in Fig. 1, which consists of a patterned metallic strip and a dielectric layer on top of a metallic ground plane. The repeat period is  $P = P_x = P_y = 60 \mu\text{m}$ . The length and width of the patterned metallic strip are  $l = 40 \mu\text{m}$  and  $w = 10 \mu\text{m}$ , respectively. The thickness of the dielectric slab is set to  $d = 5 \mu\text{m}$  in order to optimize the impedance matching of the air-structure interface, and the thickness of the patterned metal (Au) is  $t = 0.4 \mu\text{m}$  with a frequency independent conductivity of  $\sigma = 4.09 \times 10^7 \text{ S/m}$ . The dielectric constant of the dielectric is  $\varepsilon = 3(\varepsilon_1 + i\varepsilon_2)$ , where the  $\varepsilon_1 = 1$ , and  $\varepsilon_2 = 0.06$ , this dielectric material is polyethylene, which is widely used in the design of metamaterial devices [7], [8]. The proposed structure is placed in a semi-finite thick silicon substrate. Our results are obtained through finite-difference time-domain (FDTD) simulations (FDTD Solutions, Version 7.5), where the periodic structures are illustrated by a normally incident plane wave with the electric field parallel to the  $x$ -axis. Perfectly matched layers (PML) are applied along the  $z$  direction and period boundary conditions in the  $x$  and  $y$  directions. The absorption,  $A$  is obtained by  $A = 1 - T - R$ , where the  $T$  (transmission) is very close to zero as the thickness of the metallic ground plane ( $2 \mu\text{m}$ ) is much larger than its skin depth, and then the absorption is calculated by  $A = 1 - R$ . The  $A$  may achieve perfect

absorption when the  $R$  (reflection) is close to zero (i.e., impedance matched to the free space).

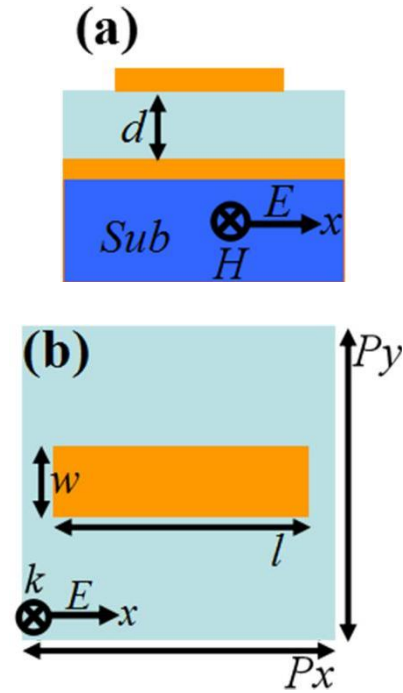


Fig. 1. Structural schematic of the proposed metamaterial absorber; (a) and (b) are respectively the side- and top-view of the unit cell (color online)

Fig. 2 shows the calculated absorption spectra of the proposed absorber. It can be seen from this figure, the absorber has a resonance absorption peak located at 2.12 THz with the absorptivity of 99.59%. The full width at half maximum with respect to the central resonance frequency is 8.5%. The large light absorption of the absorber is attributed to the coupling of the electric and magnetic resonances, and we will discuss the absorption mechanism in the next paragraph in detail. In addition, it should be noticed that the proposed structure is sensitive to the polarization state of the incident light due to the patterned metallic strip structure. Whereas a fourfold symmetric surface pattern (like square patch, square ring, cross and so on) could potentially give polarization insensitive absorption, the underlying physics of both the strip structure and fourfold symmetric patterns is essentially identical. Moreover, we investigate the origin of the loss to understand the contributions of each part of the metamaterial absorber. Fig. 2 shows the dependence of the absorption spectra on two different loss conditions (lossfree and lossy) of the dielectric layer. It can be seen from Fig. 2 that the electromagnetic energy is dissipated mostly (about 60%) in the dielectric layer of the absorber while only a small fraction is dissipated in the metal layer. This makes it less sensitive to the conducting properties of the metal surfaces, which are harder to control.

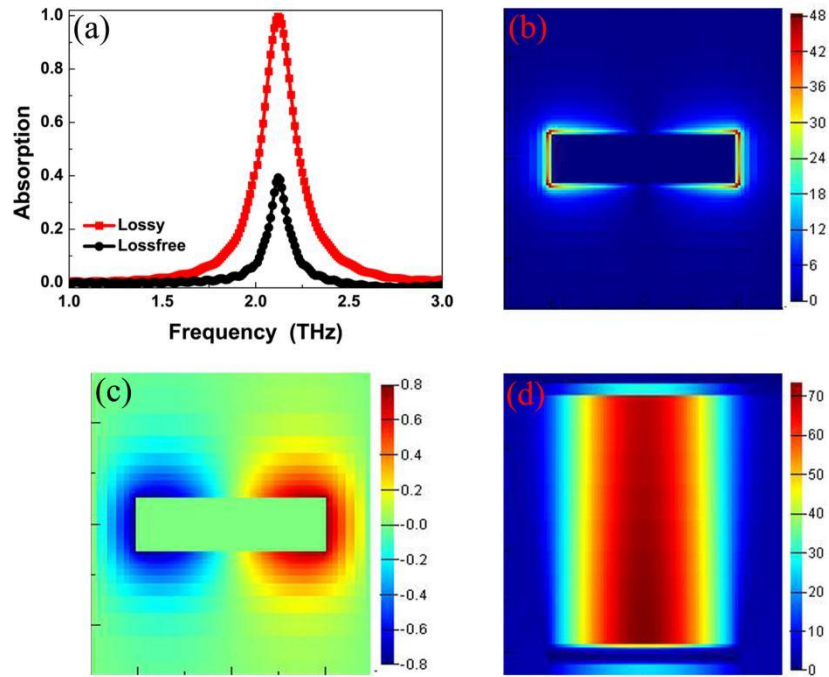


Fig. 2. (a) Simulated absorption spectra of the proposed metamaterial absorber with different loss conditions (lossfree and lossy); (b) and (c) show the distributions of the electric field ( $|E|$ ) and real ( $E_z$ ) in the center plane of the patterned metallic strip at frequency of 2.12 THz, respectively; (d) The magnetic field ( $|H_y|$ ) in the plane  $y = 0$  distribution for the proposed absorber at the frequency of 2.12 THz (color online)

To better understand the physical origin of the proposed absorber, we give the calculated electric ( $|E|$  and real ( $E_z$ ), in the center plane of the patterned structure) and magnetic ( $|H_y|$ , in the plane of  $y = 0$ ) fields distribution corresponding to the absorption maximum in Figs. 2(b)-(d). As shown in Fig. 2(b), it is obvious that the distribution of the electric field ( $|E|$ ) is mainly focused on both sides of the patterned metallic strip. The great enhancement of the electric field ( $|E|$ ) in the patterned metallic strip indicates that the larger charge accumulates at the edges of the patterned metallic strip. Thus, the distribution of the charges is mainly focused on both sides of the patterned metallic array [22], [37], [38]. As shown in Fig. 2(c), it is obvious that the opposite charges accumulate at both sides of the metallic strip (along the direction of the electric field). In fact, the distribution of the opposite charges accumulate at both sides of the metallic strip indicates the excitation of the electric dipole resonance in the patterned metallic array. This electric dipole is strongly coupled with the bottom metallic layer (i.e., its own image), and an anti-parallel surface current on the top and bottom metallic layers can be obtained. As a result, a magnetic polariton is formed, which induces a strong magnetic resonance (see the distribution of the magnetic field ( $|H_y|$ ) in Fig. 2(d)). The coupling strength of the electric dipole as well as the magnetic response is mainly determined by the thickness of the dielectric layer. By tuning the dielectric layer thickness, we can obtain an optimal value  $d = 5 \mu\text{m}$ , at which the electric and magnetic responses make the proposed structure impedance matched the free space, and a perfect absorption is obtained, as shown in the red line of the Fig. 2(a). Thus, the proposed absorber is attributed to the coupling of the

electric and magnetic resonances. Furthermore, according to the LC circuit model, the resonance frequency of the absorber is given by:  $f = \frac{1}{2\pi\sqrt{L(C_m + C_e)}}$ , where  $L$

is the inductance,  $C_m$  is the capacitance between the patterned metallic strip and the metallic ground plane, and  $C_e$  is the capacitance from the strip gap [39]. Since the electric field ( $|E|$ ) is mainly focused on the edges of the metallic strip (see Fig. 2(b)), the effective length for capacitance is reduced to  $s \cdot l$  (where  $s$  in the range of  $0.2 \leq s \leq 0.3$ ). As shown in Fig. 2(a), the resonance frequency of the absorber is calculated to be  $f = 2.11$  THz, which is consistent with the simulation result (2.12 THz), using the

$$\text{formula: } L = \mu_0 \frac{dl}{w}, \quad C_m = \frac{0.2l\epsilon_1 w}{d}, \quad \text{and} \\ C_e = \frac{\pi\epsilon_1 w}{\ln(b/d)} \approx 0.1C_m \text{ [39].}$$

### 3. Geometrical effects on the resonance frequencies

It is worth noting that, in practice, it is inevitable that there are deviations from the optimal geometric parameters in device fabrication, such as the length change of the patterned metallic strip, the thicknesses change of the dielectric layer and the metallic ground plane layer, which will reshape the absorption performance of the absorber. Therefore, in this Section, we will systematically study the dependence of the absorption spectra on the

parameters change of the absorber. In each case, only one parameter can be changed and the others are kept constant. To facilitate the investigate, we put the geometrical parameters change into three categories: (a) the parameters change of the metallic layer; (b) the parameters change of the dielectric layer; and (c) the parameters change of the unit cell.

### 3.1. The parameters change of the metallic layer

Fig. 3 (a) shows the dependence of the absorption spectra on the length change of the patterned metallic strip. It can be seen from Fig. 3(a) that a significant red-shift of the resonant absorption peak (with little change in amplitude) is obtained when the length of the patterned metallic strip increases from  $36 \mu\text{m}$  to  $44 \mu\text{m}$ . The linear dependence of the resonance frequency on the length  $l$  is demonstrated in Fig. 3(b). Since the inductance  $L$  and capacitance  $C_m$  are both proportional to the patterned metallic strip length  $l$ , the frequency of the absorber is inversely proportional to the length of the patterned metallic strip, which is consistent with the results reported in previously references [10]-[18]. On the other hand, it is found that the resonance frequency of the absorber is also sensitive to the width  $w$  of the patterned metallic strip

(while its amplitude has a neglected change), as shown in Figs. 3(c) and (d). As the strip width increases, the inductance ( $L$ ) decreasing and the capacitance  $C_m$  increasing, while the value of the  $LC_m$  does not change. The remaining capacitance  $C_e$  is proportional to the strip width  $w$ , which makes the frequency of the absorber move to lower frequencies. Additionally, it is noteworthy that the change speed of the resonance frequency for the changes of the metallic strip length  $l$  and width  $w$  is different, as shown in Figs. 3(b) and (d). The frequency change speed for the length change is larger than (about 3.5 times) that of the width change. This is why the researchers generally choose the combination of different lengths of the sub-unit to achieve the multi-band or broadband absorbers. In Section IV, we propose a novel broadband absorber by combining two different widths of patterned metallic strips. The full width at half maximum of the device is greatly improved to 27.1%, which is 3.2 times greater than that of a single-band structure. The two patterned metallic strips resonating at different but similar resonance frequencies leads to the broadband absorption. Particularly, the resonance frequency of each absorption peak can be flexible controlled by varying the width of the corresponding metallic strips. Please see the details in Section IV.

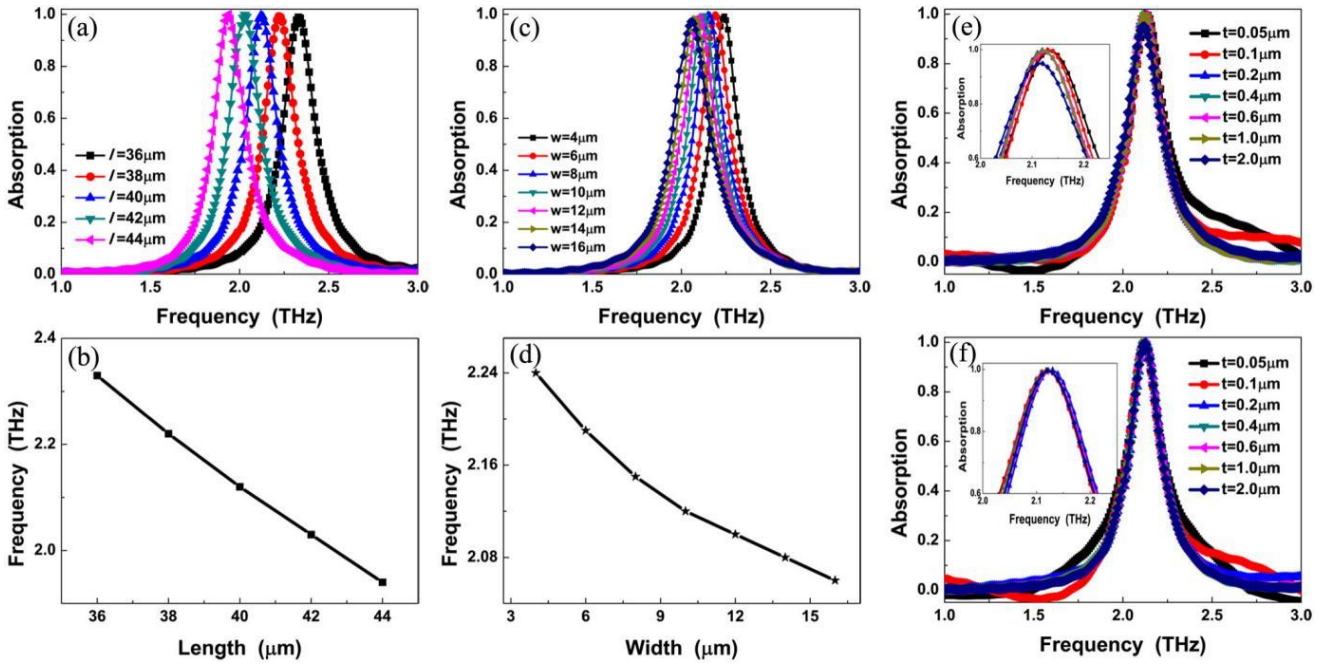


Fig. 3. Dependence of the absorption spectra on the length (a), width (b), thicknesses of the patterned (e) and the metallic ground plane (f) changes of the proposed absorber; Resonance frequencies of the proposed absorber as the functions of the length (b) and width (d); The insets of Figs. 3(e) and (f) show the dependence of the absorption spectra on the thicknesses change of the patterned structure and the metallic ground plane, respectively (color online)

Figs. 3(e) and (f) show the dependence of the absorption spectra on the thicknesses change of the patterned structure and the metallic ground plane layer, respectively. It can be seen from Figs. 3(e) and (f) that the dependence of the absorption spectra on the thicknesses change of the patterned structure and the metallic ground plane layer has a neglected change, even the thicknesses

(50 nm) of them are less than that of the skin depth of the metal. The skin depth for metal is calculated using

$$\delta = \frac{1}{\sqrt{f\pi\sigma\mu_0}}$$

where the  $f$  is the frequency,  $\mu_0$  is the vacuum permeability, and the  $\sigma$  is the conductivity of the metal [40]. Therefore, the skin depth of the Au in 2.12

THz is 54 nm. The calculated results show that not only the dependence of the absorption performance on the thicknesses change of the patterned structure and the metallic ground plane layer has a neglected change but also help us to reduce the use of the metal materials and shorten the construction time as well as cost of the device.

In some references, for example Ref. 31, the discrepancies of the experiments and simulations are attributed to the slightly different in the metallic conductivity  $\sigma$ . In this paragraph, we investigate the dependence of the absorption spectra on the change of the metallic conductivity  $\sigma$  (see below Fig. 5(b)). It is noteworthy that the conductivity change of the metallic layer does not significantly influence the absorption properties of the absorber even its conductivity ( $\sigma = 1 \times 10^6$  S/m) is reduced to one fortieth of the maximum value ( $\sigma = 4.09 \times 10^7$  S/m). Fig. 5(b) shows the calculated absorption spectra for different  $\sigma$ . It is obvious that the resonance frequency of the absorber keeps constant for different  $\sigma$ , as shown in the inset of the Fig. 5(b). Also, the absorptivity is greater than 95% as the metallic conductivity ( $\sigma = 2.5 \times 10^6$  S/m) is reduced to one sixteenth of the maximum value, and varies slightly. This absorption feature makes it less sensitive to the conductivity properties of patterned structure and the metallic ground plane layer, and

increases the choice of the metallic materials, like Au, Ag, and Cu.

### 3.2. The parameters change of the dielectric layer

As discussed above, the coupling strength of the electric dipole and the magnetic resonance is mainly determined by the dielectric layer thickness  $d$ . Therefore, the absorption performance of the absorber, in particular the absorption strength of the absorber should be sensitive to the thickness change of the dielectric layer. As shown in Fig. 4(b), it is obvious that the influence of the different thickness of the dielectric layer on the strength of the absorption indeed is sensitive. Furthermore, it is found that besides the significant dependence of the absorption strength on the change of the dielectric thickness  $d$ , a prominent frequency shift is also unveiled, as shown in Figs. 4(a) and (b). In fact, as the dielectric layer thickness  $d$  increases, the inductance ( $L$ ) increasing and the capacitance  $C_m$  decreasing, but the value of the  $LC_m$  keeps constant. The remaining capacitance  $C_e$  is proportional to the dielectric layer thickness  $d$ , and thus leads to the frequency of the absorber move to lower frequencies (or a significant red-shift is obtained, see Fig. 4(b)).

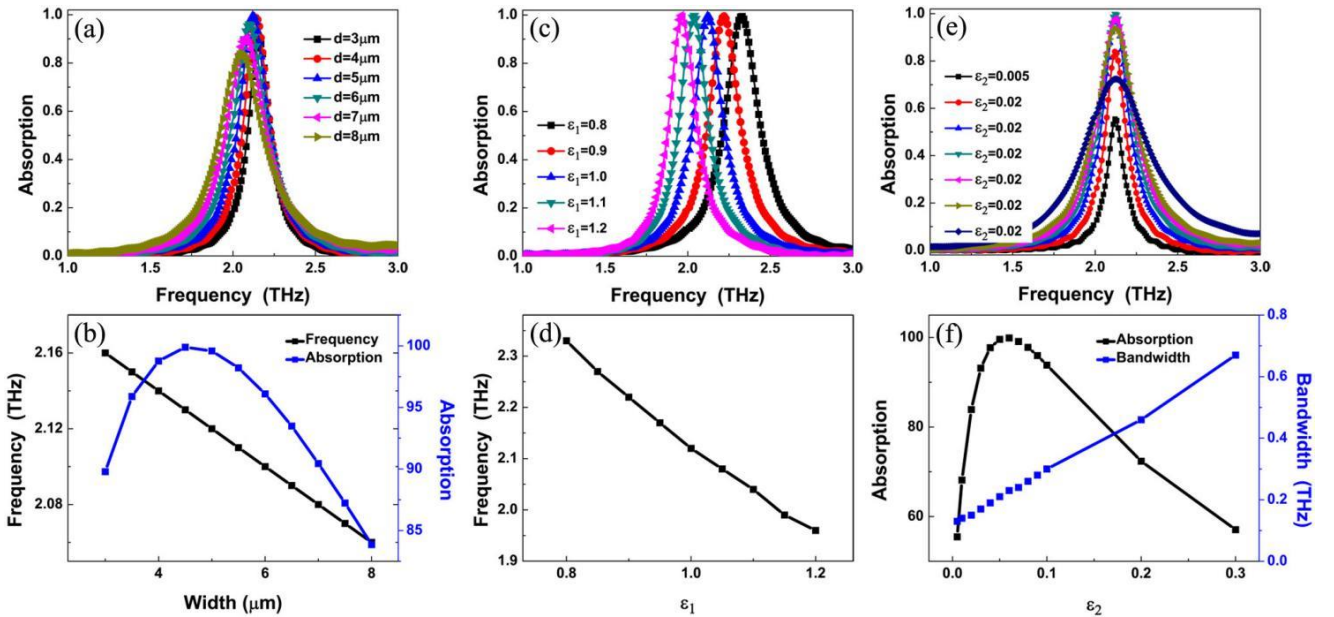


Fig. 4. (a), (c) and (e) show the dependence of the absorption spectra on the changes of the dielectric thickness  $d$ , real part  $\epsilon_1$  and imaginary part  $\epsilon_2$ , respectively; (b) Resonance frequencies and absorption of the proposed absorber as the function of the dielectric thickness  $d$ ; (d) Resonance frequencies of the absorber as the function of the  $\epsilon_1$ ; (f) Resonance frequencies and the absorption bandwidth of the proposed absorber as the function of the  $\epsilon_2$  (color online)

Fig. 4(c) shows the dependence of the absorption spectra on the real part ( $\epsilon_1$ ) change of the dielectric layer. It can be seen from Figs. 4(c) and (d) that the frequency of the absorber decreases gradually with the increase of the  $\epsilon_1$ , while its absorptivity has a slightly variation. The shift of the frequency towards longer wavelengths is explained by the increase in the effective permittivity of the dielectric layer. Larger permittivity (or real part ( $\epsilon_1$ )) of the dielectric layer gives larger resonance wavelength, and thus leads to

the decrease of the resonance frequency. Compared with the speed change of the resonance frequency in the length dependence (see Fig. 3(b)), it is obvious that the frequency change speed for the real part ( $\epsilon_1$ ) dependence is larger than that of the strip length change. Therefore, in Section IV, we present a novel broadband metamaterial absorber (i.e., the third kind of the broadband absorber) based on the real part ( $\epsilon_1$ ) change of the dielectric layer. Please see the details in Section IV.

It is noteworthy that the imaginary part ( $\epsilon_2$ ) of the dielectric layer distinctly influences the absorption properties (absorption strength and the resonance bandwidth) of the absorber. Fig. 4(e) shows the dependence of the absorption spectra on the  $\epsilon_2$  change of the dielectric layer. As shown in Figs. 4(e) and (f), it is obvious that the dielectric loss ( $\epsilon_2$ ) of the dielectric layer has a great effect on the absorption strength and the bandwidth of the absorber, while its resonance frequency has a neglected change. Specifically, the absorption strength of the absorber with the increase of the  $\epsilon_2$  has two different behaviors: a rapid enhancement and a decrease gradually (see Fig. 4(f)). First, the absorption is rapidly enhanced to an optimal value of 99.59% when  $\epsilon_2$  increases from 0.005 to 0.06. And then, the absorption decreases gradually with the further increase of the  $\epsilon_2$ . Different from the variation trend of the absorption strength, the bandwidth of the absorber increases gradually with the increase of the  $\epsilon_2$  (see Fig. 4(f)). These results suggest that dielectric loss ( $\epsilon_2$ ) of the dielectric layer has a great effect on the absorption strength and the bandwidth of the absorber, and thus we can control effectively the

properties of the absorber, in particular the absorption strength of the absorber by optimizing the  $\epsilon_2$ , which can be optimized by the chosen the dielectric materials.

### 3.3. The parameters change of the unit cell

The size of the period  $P$  is critical to tune the frequency of the absorber because the changes in the period  $P$  can significantly influence the interaction of the neighboring cells and consequently tune the bandwidth and frequency of the absorber. However, in this proposed structure, the electric field ( $|E|$ ) mainly focused on both sides of the patterned metallic strip (see Fig. 2(b)), which makes the interaction of the neighboring cells very weak. Thus, we consider that the influence of the period  $P$  (in a small range of variation) on the resonance frequency and absorption bandwidth should be relatively weak. Fig. 5 shows the calculated absorption spectra for different period  $P$ . It can be seen from Fig. 5(a) that the dependence of the absorption spectra on the change of the period  $P$  indeed is weak.

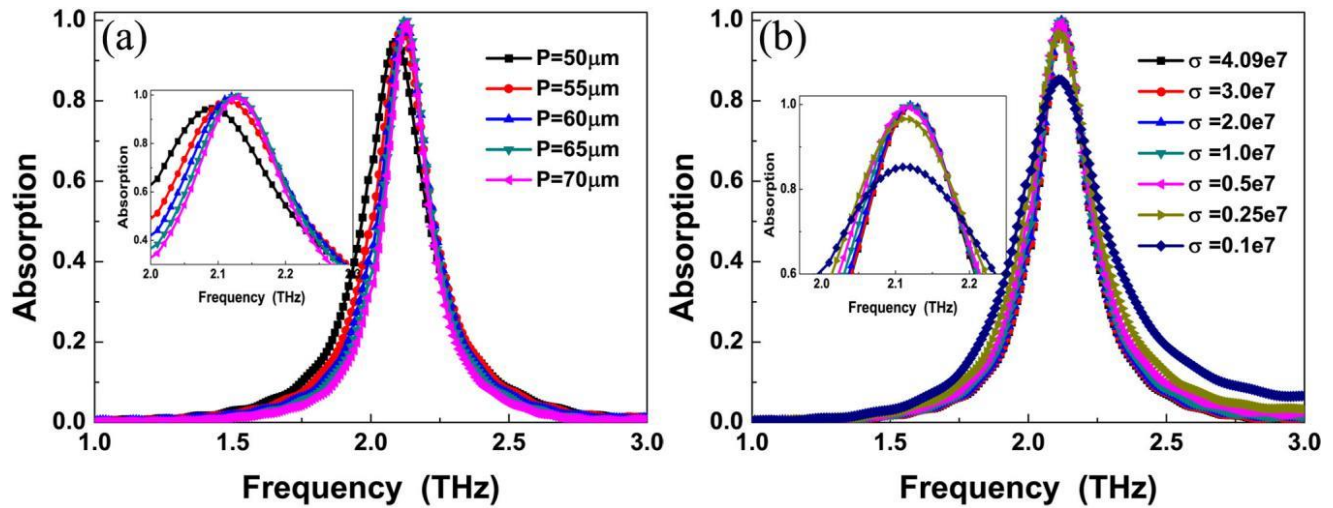


Fig. 5. (a) and (b) show the dependence of the absorption spectra on the changes of the period  $P$  and of the metallic conductivity  $\sigma$ , respectively; The insets of the Figs. 5(a) and (b) show the dependence of the absorption spectra on the changes of the  $P$  and  $\sigma$ , respectively (color online)

We can conclude that the influence of the parameters on the performance of the absorber can be divided into three categories: (a) the length  $l$  and width  $w$  of the patterned metallic strip, the real part ( $\epsilon_1$ ) of the dielectric constant and the thickness  $d$  of the dielectric layer mainly influence the frequency of the absorber; and (b) the change of the absorptivity mainly depends on the imaginary part ( $\epsilon_2$ ) of the dielectric constant and the thickness  $d$  of the dielectric layer; while (c) the influence of the metallic conductivity  $\sigma$ , the thicknesses  $t$  of the patterned structure and the metallic ground plane layer as well as the period  $P$  of the unit cell on the performance (resonance frequency and absorption strength) of the absorber is negligible.

In this paragraph, we employ the results obtained in Sections III to explain the discrepancies between the

experiments and simulations. As shown in Fig. 3(c) in Ref. 31, it is obvious that the measured absorption bandwidth has a slightly broadening compared with the simulations, while the changes of the resonance frequency and the absorption strength are negligible. The broadened absorption bandwidth is attributed to slightly different in the metallic conductivity and dielectric loss of the dielectric layer [31]. As discussed above, however, the influence of the metallic conductivity on the performance of the absorber has a neglected change even its conductivity reduces to one sixteenth of the maximum value. Thus, the slightly broadening of the absorption bandwidth originates from the dielectric loss of the dielectric layer. Furthermore, according to the variation trend of the absorption bandwidth: the bandwidth of the absorber increases gradually with the increase of the  $\epsilon_2$ .

(see Fig. 4(f)), thus we think that the dielectric loss of the dielectric layer should be slightly increased. As another example, it can be seen from Fig. 3 in Ref. 20 that the measured three resonance frequencies are all slightly different from the simulations, while there are almost no changes in strength of absorption. Therefore, these discrepancies are attributed to the lengths change of the nested electric closed-ring resonators. Specifically, the lengths of the  $L1$  and  $L2$  are both slightly increase because the measured frequencies for these two lower absorption peaks are less than that of the simulations, while the length of the  $L3$  should be slightly decreased due to the measured the highest resonance frequency is larger than that of the simulation value.

#### 4. Design of broadband absorption

Below we try to increase the bandwidth of the absorption by using a stacked structure which can support several resonance absorption peaks closely positioned in the absorption spectra. As discussed above, the frequency of the absorber can be tuned by the length  $l$  and width  $w$  of the patterned metallic strip, and real part ( $\epsilon_1$ ) of the dielectric constant. Thus, multiple metallic strips with different geometrical parameters (different lengths  $l$  and different widths  $w$ ) or same-sized geometrical parameters but each layer with different dielectric constants are positioned on a stacked structure to ensure that the resonance frequencies could be close to each other. Then, by tuning the dielectric separation thickness of each layer, the stacked structure can be impedance matched to the free space at each resonance frequency. Figs. 6(a) and (b) show the cross sections of the proposed double-layered absorber.

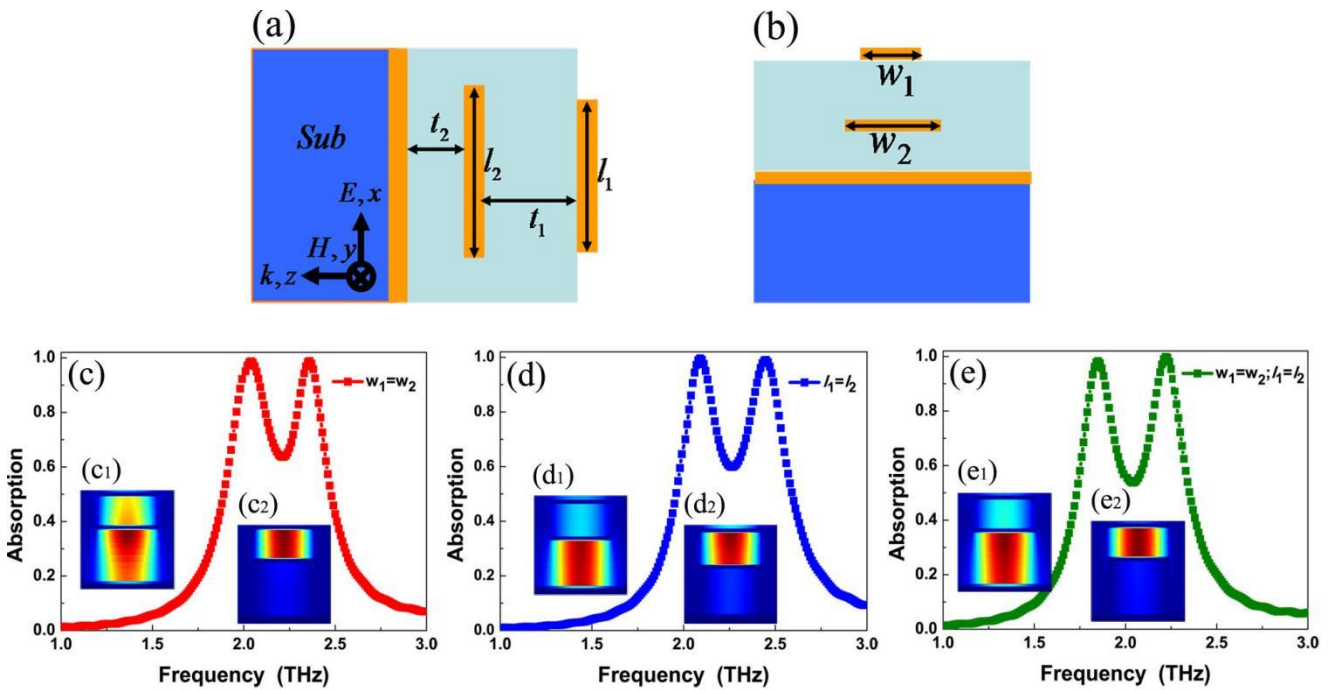


Fig. 6. (a) and (b) show the cross section of the proposed broadband absorber; (c), (d) and (e) show the dependence of the absorption spectra for the proposed first, second and third kinds of broadband absorbers, respectively; (c1) and (c2) show the distributions of the magnetic field ( $|H_y|$ , in the plane  $y = 0$ ) for the proposed the first kind of the broadband absorber at the frequencies of 2.09 THz and 2.45 THz, respectively; (d1) and (d2) show the distributions of the magnetic field ( $|H_y|$ , in the plane  $y = 0$ ) for the proposed the second kind of the broadband absorber at the frequencies of 2.04 THz and 2.36 THz, respectively; (e1) and (e2) show the distributions of the magnetic field ( $|H_y|$ , in the plane  $y = 0$ ) for the proposed the third kind of the broadband absorber at the frequencies of 1.85 THz and 2.22 THz, respectively (color online)

For the sake of clarify, we first study the case of the different lengths metallic strips. The cross sections of the considered broadband absorber are depicted in Figs. 6(a) and (b). The optimal parameters of the proposed absorber are followed in micrometers:  $P = P_x = P_y = 60$ ,  $l_1 = 38$ ,  $l_2 = 40$ ,  $w_1 = w_2 = 6$ ,  $t_1 = 3$ ,  $t_2 = 5.5$ . The conductivity and thickness of the metal (Au), and the dielectric constant of the dielectric are the same in the single-band absorber. Fig. 6(c) shows the calculated absorption spectra of the proposed broadband absorber. Different from the case of the single-band absorber with single resonance absorption

peak, the proposed broadband absorber has two resonance frequencies, located at the frequencies of 2.09 THz ( $f_1$ ) and 2.45 THz ( $f_2$ ) with the absorption strength of 99.61% and 99.02%, respectively. Owing to these two closely positioned resonance absorption peaks we obtain a wide frequency band, from 1.97 THz to 2.59 THz, where the absorption is greater than 50%. If we take the central frequency of the broadband resonance as 2.27 THz, the larger than 50% relative absorption bandwidth of the device is improved to 27.3%, which is 3.2 times larger than that of the single-band absorber.

To reveal the physical origin of the spectral characteristics, the distributions of the  $y$ -component magnetic field ( $H_y$ ) in the plane  $y = 0$  corresponding to two absorption maximum are shown in Figs. 6(c<sub>1</sub>) and (c<sub>2</sub>). Different field distributions are observed for the frequencies at 2.09 and 2.45 THz. As shown in Fig. 6(c<sub>1</sub>), the resonance at 2.09 THz ( $f_1$ ) is primarily associated with the excitation of the bottom patterned metallic layer (i.e., the magnetic field is mainly focused on the dielectric layer  $t_2$ ), while the resonance at 2.45 THz ( $f_2$ ) is mainly a consequence of excitation of the top patterned metallic layer (i.e., the magnetic field is mainly focused on the dielectric layer  $t_1$ ) (see Fig. 6(c<sub>2</sub>)). Obviously, the combination of those two absorption peaks determines the broadband absorption.

With the mechanism of the broadband absorption having been explained, the influence of parameters on the frequencies and bandwidth can be easily understood. As discussed above, the frequency of the absorber mainly

depend on the length of the patterned metallic strip. Thus, with other parameters fixed, the length change of the patterned metallic array can significantly influence the frequencies  $f_1$  and  $f_2$  and consequently tune the bandwidth of the absorber. Figs. 7(a) and (b) show the influence of the lengths of  $l_1$  and  $l_2$  on the resonance frequencies and absorption bandwidth, respectively. It is obvious that as the length  $l_1$  is increased,  $f_2$  becomes small while the mode  $f_1$  is nearly fixed, which results in the increase of the absorption bandwidth (see Fig. 7(a)). Similarly, for the change of the  $l_2$ , the  $f_1$  gradually increases with the decrease of the  $l_2$  (see Fig. 7(b)), while the change of the mode  $f_2$  is neglected. Obviously, the changes of the  $l_1$  and  $l_2$  provide the ability to shift or even broaden the absorption bandwidth. However, the changes of the  $l_1$  and  $l_2$  cannot be too large because the proposed absorber cannot be considered as the broadband absorber and becomes a dual-band absorber (or the frequencies  $f_1$  and  $f_2$  are far apart, see Figs. 7(a) and (b)).

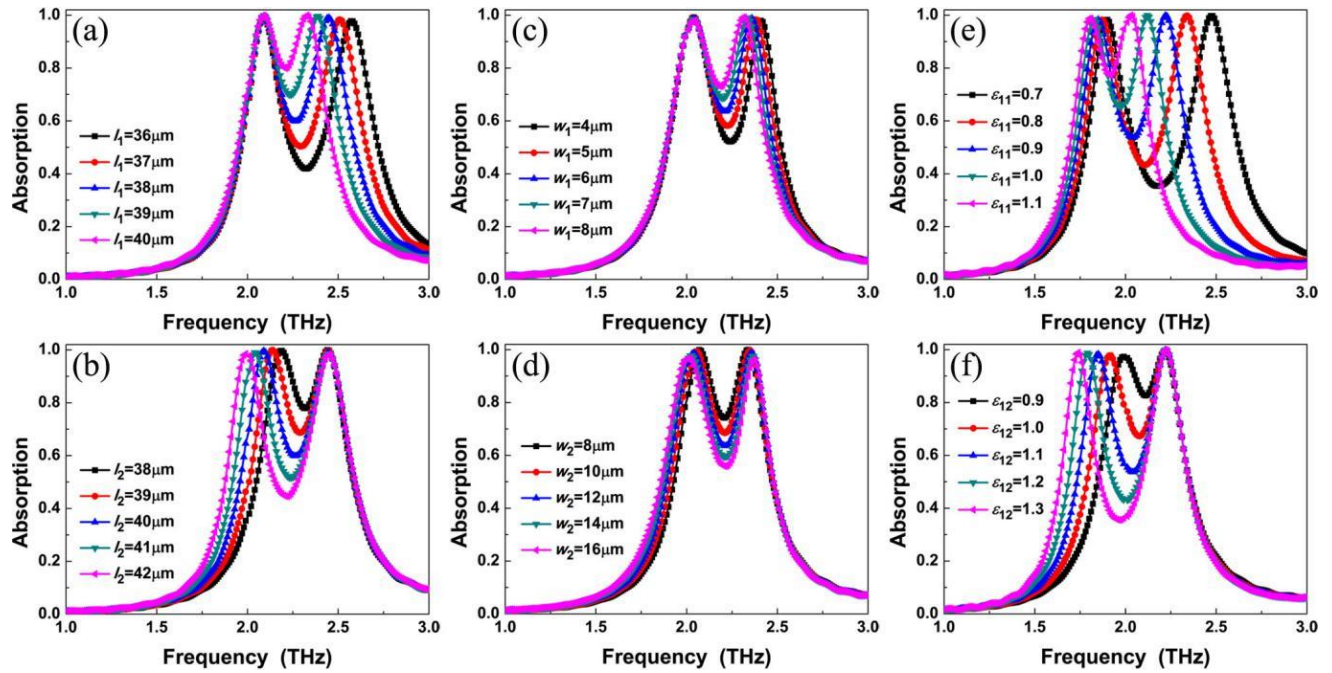


Fig. 7. Dependence of the absorption spectra on the length changes of the  $l_1$  (a) and  $l_2$  (b) for the proposed the first kind of the broadband absorber; Dependence of the absorption spectra on the width changes of the  $w_1$  (c) and  $w_2$  (d) for the proposed the second kind of the broadband absorber; Dependence of the absorption spectra on the real part changes of the  $\epsilon_{11}$  (e) and  $\epsilon_{12}$  (f) for the proposed the third kind of the broadband absorber (color online)

The broadband absorption can be alternatively obtained by changing the widths of the patterned metallic strips. The unit cell of the proposed structure is shown in Figs. 6(a) and (b), the optimal parameters of the structure are followed in micrometers:  $P = P_x = P_y = 60$ ,  $l_1 = l_2 = 40$ ,  $w_1 = 6$ ,  $w_2 = 12$ ,  $t_1 = 3.5$ ,  $t_2 = 5$ . The conductivity of the metal (Au) and the dielectric constant of the dielectric are the same shown in Fig. 1. Fig. 6(d) shows the calculated absorption spectra of the proposed broadband absorber. It can be seen from Fig. 6(a) that the absorption spectra consists of two resonance absorption peaks located at 2.04 THz and 2.36 THz, each with absorptions over 98.80%. The relative absorption bandwidth of the device (i.e.,

greater than 50% absorption) is 27.1%, which is 3.2 times larger than that of the single-band absorber. Furthermore, the distributions of magnetic field in the plane  $y = 0$  corresponding to two absorption maximum are shown in Figs. 6(d<sub>1</sub>) and (d<sub>2</sub>). It can be seen from Figs. 6(d<sub>1</sub>) and (d<sub>2</sub>) that the distributions of the magnetic field for the different widths absorber are similar to that of the different lengths broadband absorber (see Figs. 6(c<sub>1</sub>) and (c<sub>2</sub>)). Therefore, the mechanism of the broadband absorber is attributed to the combination of two different but similar resonance frequencies.

The above-mentioned two kinds of broadband absorbers are based on vertically stacking two

metal/dielectric layers with different geometrical dimensions. In fact, the dielectric spacing layer, especially its dielectric constant, is a vital but often overlooked factor in designing the broadband absorber. Therefore, in this paragraph, we propose a novel broadband absorber (i.e., the third kind of the broadband absorber) based on two same-sized metallic strips but each layer with different dielectric constants. The cross sections of the considered broadband absorber are depicted in Figs. 6(a) and (b). The optimal parameters of the proposed broadband absorber are followed in micrometers:  $P = P_x = P_y = 60$ ,  $l_1 = l_2 = 40$ ,  $w_1 = w_2 = 10$ ,  $t_1 = 3$ ,  $t_2 = 5.5$ . The conductivity and thickness of the metal (Au) are the same in the single-band absorber. The dielectric constants of the dielectric in layers  $t_1$  and  $t_2$  are  $3(\epsilon_{11} + i0.06)$  and  $3(\epsilon_{12} + i0.06)$ , respectively, where the  $\epsilon_{11} = 0.9$  and  $\epsilon_{12} = 1.1$ . Fig. 6(e) shows the calculated absorption spectra of the proposed broadband absorber. It can be seen from Fig. 6(e) that the proposed broadband absorber has two resonance frequencies, located at the frequencies of 1.85 THz ( $f_1$ ) and 2.22 THz ( $f_2$ ) with the absorption strength of 98.23% and 99.87%, respectively. Taking the central frequency of the broadband resonance as 2.04 THz, the greater than 50% relative absorption bandwidth of the device is greatly improved to 30.5%, which is 3.6 times larger than that of the single-band absorber.

To better understand the physical origin of the broadband absorption, we give the calculated magnetic field ( $|Hy|$ ) distributions (in the plane  $y = 0$ ) corresponding to two absorption maximum in Figs. 6(e<sub>1</sub>) and (e<sub>2</sub>). As shown in Fig. 6(e<sub>1</sub>), the resonance at 1.85 THz ( $f_1$ ) is mainly a consequence of excitation of the bottom patterned metallic layer (i.e., the dielectric layer  $t_2$ , where its dielectric constant is larger than that of the dielectric layer  $t_1$ ), while the resonance at 2.22 THz ( $f_2$ ) is primarily associated with the excitation of the top patterned metallic layer (i.e., the dielectric layer  $t_1$ ). These distributions clearly reveal that each patterned metallic strip contributes to the broadband absorption. Furthermore, the design gives a considerable freedom to shift or even broaden the absorption band by independently changing the dielectric constants ( $\epsilon_{11}$  and  $\epsilon_{12}$ ) of each dielectric layer (see Figs. 7(e) and (f)), which is similar to the results obtained in Figs. 7(a) and (b).

## 5. Conclusion

In conclusion, we study the dependence of the absorption performance on the parameters change of the absorber consisted of a patterned metallic strip and a metallic ground plane separated by a dielectric layer. The influence of the parameters on the performance of the absorber can be divided into three categories: (a) the frequency of the absorber mainly depends on the length and width of the patterned metallic strip, the real part of the dielectric constant and the thickness of the dielectric layer; (b) the thickness of the dielectric layer and the imaginary part of the dielectric constant mainly influence the absorptivity of the absorber; while (c) the influence of

the metallic conductivity, the thicknesses of the patterned and the ground plane metallic layers, and the period of the unit cell on the performance of the absorber is negligible. We believe that the systematically study of the influence of the parameters on the performance of the absorber can provide a useful guide to understand and optimize the absorber and also explain the discrepancy between the measurements and the simulations. Moreover, we present three kinds of broadband absorbers based on the results obtained in (a). The absorption bandwidth with respect to the central resonance frequency of those three absorber devices is greatly improved to 27%, which is 3.2 times larger than that of the single-band absorber. The mechanism of the three kinds of the broadband absorber is attributed to the combination of two different but similar resonance frequencies. Such broadband terahertz metamaterial absorbers have potential applications as a functional THz thermal detector or stealth technology.

## Acknowledgments

This research was funded by National Natural Science Foundation of China (21603087, 11647143), Natural Science Foundation of Jiangsu (BK20160178, BK20160189), China Postdoctoral Science Foundation (2019M651692), Jiangsu Postdoctoral Science Foundation (2018K113C), Fundamental Research Funds for Central Universities (JUSRP51721B).

## References

- [1] W. Cai, U. K. Chettiar, A. V. Kildishev, V. M. Shalaev, *Nat. Photon.* **1**, 224 (2007).
- [2] G. Rosenblatt, M. Orenstein, *Phys. Rev. Lett.* **115**, 195504 (2015).
- [3] R. A. Shelby, D. R. Smith, S. Schultz, *Science* **292**, 77 (2001).
- [4] S. Jahani, Z. Jacob, *Nat. Nanotechnol.* **11**, 23 (2016).
- [5] C. D. Giovampaola, N. Engheta, *Nat. Mater.* **13**, 1115 (2014).
- [6] N. I. Landy, S. Sajuyigbe, J. J. Mock, D. R. Smith, W. J. Padilla, *Phys. Rev. Lett.* **100**, 207402 (2008).
- [7] L. Huang, D. R. Chowdhury, S. Ramani, M. T. Reiten, S. N. Luo, A. K. Azad, A. J. Taylor, H. T. Chen, *Appl. Phys. Lett.* **101**, 101102 (2012).
- [8] N. K. Grady, J. E. Heyes, D. R. Chowdhury, Y. Zeng, M. T. Reiten, A. K. Azad, A. J. Taylor, D. A. R. Dalvit, H. T. Chen, *Science* **340**, 1304 (2013).
- [9] R. Kumar, S. A. Ramakrishna, *J. Nanophoton.* **14**, 016011 (2020).
- [10] Y. Liao, Y. Zhao, *Sci. Rep.* **10**, 1480 (2020).
- [11] I. Ozbay, A. Ghobadi, B. Butun, G. Turhansayan, *Opt. Lett.* **45**, 686 (2020).
- [12] H. Huang, H. Xia, Z. Guo, D. Xie, H. Li, *Appl. Phys. A* **124**, 429 (2018).
- [13] B. X. Wang, C. Tang, Q. Niu, Y. He, T. Chen, *Nanoscale Res. Lett.* **14**, 64 (2019).

- [14] H. Huang, H. Xia, Z. Guo, H. Li, D. Xie, *Opt. Commun.* **424**, 163 (2018).
- [15] H. Huang, H. Xia, W. Xie, Z. Guo, X. Li, D. Xie, *Sci. Rep.* **8**, 4183 (2018).
- [16] D. Li, H. Huang, H. Xia, Z. Guo, J. Zeng, H. Li, D. Xie, *Results Phys.* **11**, 659 (2018).
- [17] J. Gou, T. Zhang, J. Wang, Y. Jiang, *Nanoscale Res. Lett.* **12**, 91 (2017).
- [18] Y. Cui, J. Xu, K. H. Fung, Y. Jin, A. Kumar, S. He, N. X. Fang, *Appl. Phys. Lett.* **99**, 253101 (2011).
- [19] S. D. Assimonis, V. F. Fusco, *Sci. Rep.* **9**, 12334 (2019).
- [20] X. Shen, T. J. Cui, J. Zhao, H. F. Ma, W. X. Jiang, H. Li, *Opt. Express* **19**, 9401 (2011).
- [21] J. Grant, Y. Ma, S. Saha, A. Khalid, D. R. S. Cumming, *Opt. Lett.* **36**, 3476 (2011).
- [22] Y. Ye, Y. Jin, S. He, *J. Opt. Soc. Am. B* **27**, 498 (2010).
- [23] Y. Zhou, Z. Shen, J. Wu, Y. Zhang, S. Huang, H. Yang, *Appl. Phys. B* **126**, 1 (2020).
- [24] A. Sharma, R. Panwar, R. Khanna, *IEEE Magnetic. Lett.* **10**, 1 (2019).
- [25] B. Appasani, P. Prince, R. K. Ranjan, N. Gupta, V. K. Verma, *Plasmonics* **14**, 737 (2019).
- [26] C. Tran, H. V. Pham, H. Nguyen, T. T. Nguyen, L. D. Vu, T. H. Do, *Plasmonics* **14**, 1587 (2019).
- [27] T. Chen, S. Li, X. Cao, J. Gao, Z. Guo, *Appl. Phys. A* **125**, 232 (2019).
- [28] B. X. Wang, Y. He, N. Xu, X. Wang, Y. Wang, J. Cao, *Results Phys.* **17**, 103077 (2020).
- [29] B. X. Wang, Y. He, P. Lou, W. Xing, *Nanoscale Adv.* **2**, 763 (2020).
- [30] B. X. Wang, Y. He, P. Lou, W. Q. Huang, F. Pi, *Results Phys.* **16**, 102930 (2020).
- [31] M. P. Hokmabadi, D. S. Wilbert, P. Kung, S. M. Kim, *Phys. Rev. Appl.* **1**, 044003 (2014).
- [32] B. X. Wang, *IEEE J. Sel. Top. Quantum Electron.* **23**, 4700107 (2017).
- [33] B. X. Wang, G. Z. Wang, T. Sang, *J. Phys. D* **49**, 165307 (2016).
- [34] B. X. Wang, G. Z. Wang, L. L. Wang, *Plasmonics* **11**, 523 (2016).
- [35] B. X. Wang, *Plasmonics* **12**, 95 (2017).
- [36] B. X. Wang, G. Z. Wang, *Plasmonics* **13**, 123 (2018).
- [37] N. Liu, L. Fu, S. Kaiser, H. Schweizer, H. Giessen, *Adv. Matter.* **20**, 3859 (2008).
- [38] N. Liu, H. Guo, L. Fu, S. Kaiser, H. Schweizer, H. Giessen, *Adv. Matter.* **19**, 3628 (2007).
- [39] J. Zhou, E. N. Economon, T. Koschny, C. M. Soukoulis, *Opt. Lett.* **31**, 3620 (2006).
- [40] R. Singh, E. Smirnova, A. J. Taylor, J. F. Ohara, W. Zhang, *Opt. Express* **16**, 6537 (2008).

---

\* Corresponding authors: wangbenxin@jiangnan.edu.cn  
pifuwei@jiangnan.edu.cn